Available online at www.sciencedirect.com
SCIENCE DIRECT®
International Journal of Heat and Mass Transfer 47 (2004) 5725–5739
International Journal of HEAT and MASS TRANSFER
www.elsevier.com/locate/ijhmt

Gas–liquid two-phase flow patterns in a miniature square channel with a gas permeable sidewall

H. Yang, T.S. Zhao *, P. Cheng

Department of Mechanical Engineering, The Hong Kong University of Science and Technology, Clear Water Bay, Kowloon, Hong Kong, China

Received 3 February 2004; received in revised form 28 June 2004
Available online 16 September 2004

Abstract

Characteristics of air–water two-phase flow patterns in a miniature square channel having a gas permeable sidewall were investigated experimentally. Water was fed into the channel from its entrance, while air was injected uniformly into the channel along the permeable sidewall. This configured two-phase flow problem is encountered in direct feed methanol fuel cells. Flow patterns in both vertical upward and horizontal flows were identified using a high-speed motion analyzer. The visualization shows that the typical flow pattern encountered in the conventional co-current gas–liquid two-phase flow, such as bubbly flow, plug flow, slug flow and annular flow were also observed in the present work. However, unlike the conventional co-current gas–liquid two-phase flow in a channel with gas and liquid uniformly entering from one of its ends, for the flow configuration considered in this work, the stratified flow and wavy flow were not found in horizontal flow. And a so-called "single layer bubbly flow" was found in vertical upward flow, which is characterized by a mono small-gas-bubble layer existing adjacent to the surface of the permeable sidewall with the reminding space occupied by the liquid phase. Four transitional flow patterns such as bubbly-plug flow, bubbly-slug flow, plug–slug flow, and slug-annular flow, were found to exist between the distinct flow patterns. Finally, the flow regime maps for various liquid volumetric fluxes are presented in terms of mass quality versus the volumetric flux of gas phase.

1. Introduction

Gas–liquid two-phase flow is of great importance in a wide variety of engineering fields and industries. Examples include heat transfer systems, distillation processes, steam generators, and numerous chemical industrial processes, such as continuous loop reactors, bubble column reactors, gas–liquid pipeline systems and so on. It is well known that the morphology of a two-phase flow very often plays a critical role in determining heat and mass transfer during phase-change heat transfer processes. Thus, research on the characterization of two-phase flow patterns is essential for a better understanding of the underlying mechanisms of boiling and condensation heat transfer in channels. Early studies of gas–liquid two-phase flow patterns predominantly consisted of flow in large circular tubes. For example, Hewitt and Roberts [1] studied flow patterns in vertical upward co-current flow; Alves [2] investigated flow patterns in horizontal co-current flow; Golan and Stenning [3] as well as Oshinowo and Charles [4] reported flow

* Corresponding author. Tel.: +852 2358 8647; fax: +852 2358 1543.
E-mail address: metzhao@ust.hk (T.S. Zhao).

0017-9310/$ - see front matter © 2004 Elsevier Ltd. All rights reserved.
doi:10.1016/j.ijheatmasstransfer.2004.07.025

Nomenclature

A_c	cross-sectional area of the channel, m^2
A_p	area of the porous sidewall, m^2
D_h	hydraulic diameter of the channel, m
G_f	mass velocity of liquid phase, $kg/m^2 s$
G_g	mass velocity of gas phase, $kg/m^2 s$
J_G	volumetric flux of gas air, m/s
J_L	volumetric flux of liquid water, m/s
L	the total length of the test section, m
L_x	the axial distance, m
$L_{x,e}$	end point of each flow pattern, m
$L_{x,s}$	start point of each flow pattern, m
Q_G	volumetric flow rate of gas air, m^3/s
Q_L	volumetric flow rate of liquid water, m^3/s
X	mass quality
x_{max}	the maximum value of mass quality

Greek symbols

μ	viscosity, $N s/m^2$
λ	factor defined by Eq. (8)
ρ_G	the gas density, kg/m^3
ρ_L	the liquid density, kg/m^3
σ	surface tension, N/m
ψ	factor defined by Eq. (9)

Subscripts

A	air
F	liquid phase
g	gas phase
G	gas air
L	liquid water
W	water

patterns in vertical downward flows; and Kosterin [5] and Brigham et al. [6] discussed flow patterns in inclined channels.

Recently, a number of investigations on gas–liquid two-phase flow patterns in mini-channels, with circular and non-circular cross-sections, have been reported. Damianides [7] experimentally studied the two-phase flow of air–water mixtures in horizontal pipes, the flow patterns and flow regime maps for five glass tubes having inner diameters of 5.0, 4.0, 3.0, 2.0 and 1.0 mm were determined using visualization techniques (high-speed still and motion picture photography). Mishima and Hibiki [8] studied the characteristics of air–water two-phase flow in small diameter vertical tubes. Flow regime, void fraction, rising velocity of slug bubbles, and frictional pressure drops were measured for air–water flows in capillary tubes having inner diameters ranging from 1.0 to 4.0 mm. Galbiati and Andreini [9] experimentally studied the inlet mixing effect on flow pattern transitions for vertical downward two-phase flow in capillary tubes with diameters of 0.5, 1.1, 2.0 mm, respectively. Keska and Fernando [10] experimentally studied adiabatic air–water two-phase flow in a small, horizontal, 6.35 mm square channel. Coleman and Garimella [11] investigated the effect of tube diameter and shape on the flow patterns for hydraulic diameters ranging from 5.5 to 1.3 mm. Ewing et al. [12] experimentally studied the horizontal two-phase flow patterns of air and water two-phase flows in a transparent circular channel (1.90 cm I.D.). More recently, Zhao and Bi [13] experimentally investigated co-current upward air–water two-phase flow in vertical miniature triangular channels with hydraulic diameters of 2.886, 1.443 and 0.886 mm respectively. A so-called "capillary bubbly flow pattern" was found at low gas flow rates. Triplett et al. [14] carried out the experiments on the air–water flow patterns in circular microchannels with 1.1 and 1.45 mm inner diameters, and in microchannels with semi-triangular (triangular with one corner smoothed) cross-sections with hydraulic diameters 1.09 and 1.49 mm. The gas and liquid superficial velocity ranges were 0.02–80 and 0.02–8 m/s, respectively.

Our literature review shows that all the previous works on gas–liquid two-phase flow in channels have been confined to the configuration, in which well-mixed liquid and gas entered a channel from one end and a distinct flow pattern usually occurred in the entire channel for a fixed flow rate of liquid and gas. In this work, we are concerned with a newly configured two-phase flow in a miniature square channel with a gas permeable sidewall, in which a liquid is fed into the channel from its entrance, while a gas is injected uniformly into the test channel along the permeable sidewall. The problem under consideration is encountered in the design of direct feed methanol fuel cells (DMFC).

Polymer electrolyte fuel cells have a number of features that make them an attractive power source for transportation applications. In particular, they can be operated on a direct feed of liquid methanol, which allows vehicle refueling to be no more labor intensive than a spark ignition engine that runs on gasoline. Direct methanol fuel cells (DMFC) have the advantages of convenience and simplicity of design. Furthermore, methanol is a high energy density liquid at room temperature and can be handled easily and obtained from a variety of sources.

The liquid direct methanol fuel cell, as shown schematically in Fig. 1, consists of a proton exchange membrane with an anode and a cathode catalyst layer on each side. Gas diffusion layers are used to cover the cat-

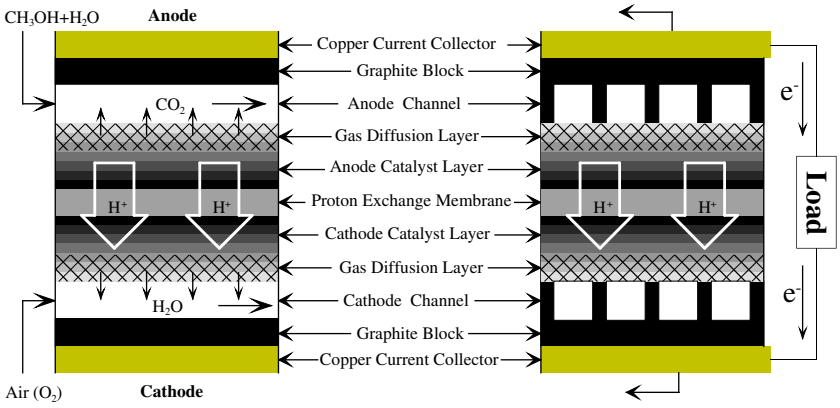

Fig. 1. Schematic of a liquid-fed direct methanol fuel cell (DMFC).

alyst layers and form the membrane electrode assembly (MEA). The MEA is then sandwiched between two current collectors that have some flow channels machined into the surface for the supply of fuel and oxidant. The liquid direct methanol fuel cell uses liquid methanol as fuel, air or oxygen as oxidant, and can be operated at a temperature lower than 100 °C. The electrochemical reactions taking place in the cell are described as follows:

$$\text{Anode side: } CH_3OH + H_2O \rightarrow 6e^- + 6H^+ + CO_2 \quad (1)$$

$$\text{Cathode side: } 3/2\,O_2 + 6e^- + 6H^+ \rightarrow 3H_2O \quad (2)$$

which can be combined to give the overall reaction as:

$$CH_3OH + 3/2\,O_2 \rightarrow 2H_2O + CO_2 \quad (3)$$

Thus, the overall cell reaction is that the methanol reacts with oxygen, producing carbon dioxide and liquid water. Apparently, all the reaction products, carbon dioxide at the anode and liquid water at the cathode, should be removed from the electrode structure and cell as efficiently as possible to maintain an effective continuous reaction. Like the water management at the cathode, the efficient removal of carbon dioxide at the anode is one of the most important research issues in the development of the liquid feed direct methanol fuel cells.

The anode side is a two-phase system primarily consisting of a methanol solution and product gas CO_2. The methanol must diffuse to the catalyst, while the reaction-generated CO_2 must diffuse outward from the catalyst. At high current densities, CO_2 can become a large volume fraction (>90%) in the anode flow field. CO_2 removal from the catalyst site is critical to ensure availability of an adequate surface area for methanol oxidation. Anode backing layers are partially coated by Teflon to aid CO_2 removal. In addition to CO_2 transport from the catalyst surface to the backing layer, CO_2 removal from the anode exit is critical. Gas slugs may form at the exit of the manifolds, resulting in high pressure drops. As a result of the higher required anode pressure, increased methanol crossover to the cathode will occur, reducing the performance. Thus, it is crucial to ensure optimal CO_2 removal, both from the backing layer and from the flow channels.

Relatively few papers have been reported on the study of bubble behavior at the anode of DFMCs. Mench et al. [15] examined gas bubble growth and ejection from the backing layer/flow channel interface region with video microscopy and observed discrete bubbles of the order of 0.1–0.5 mm evolving from various locations within the backing layer. Argyropoulos et al. [16] recorded three flow patterns including bubbly, slug and annular flow with the aid of a high-speed video camera in a practical fuel cell working environment. In their experiments, they used the design of a flow bed adopted parallel channel structure, which consisted of a series of parallel flow channels, square cross-section $2.0 \times 2.0\,mm^2$ and only 30.0 mm long. The effects of the current density and the liquid flow rate were considered. Zhao and Yang [17] reported their visualization investigation of gas–liquid flow patterns in a horizontal channel having a gas permeable sidewall. The channel was made of transparent Lucite with $5.0 \times 5.0\,mm^2$ square cross-section area and 320.0 mm in length. And the flow patterns found in their experiments included bubbly flow, plug flow, slug flow and annular flow.

Since a characterization of two-phase flow patterns is essential for a better understanding of the underlying mechanisms of a gas–liquid two-phase flow in a miniature channel having a gas permeable sidewall, we visually investigated the morphology of a gas–liquid two-phase flow in both vertical and horizontal rectangular channels with one of the sidewalls consisting of a porous plate. Liquid was fed into the test section from its entrance, while gas was injected uniformly into the test section along the porous sidewall. The results

presented in this paper are useful for the optimal design of a two-phase flow system in a channel having a permeable sidewall, for instance, the anode flow manifolds in the liquid-fed methanol fuel cells.

2. Experimental apparatus

2.1. Test section

As illustrated in Fig. 2, the test section consisted of a square channel ($5.0 \times 5.0\ mm^2$ in cross-section area and 320.0 mm in length) with one of its sidewalls permeable to gases. A channel entrance portion, 280.0 mm long, with the same cross-section area as the test section but without the permeable sidewall, preceded the test section. Water was fed into the test section from its entrance, while air was injected uniformly into the test section along the porous sidewall. For the purpose of visualization, the test section was made of transparent Lucite. The permeable sidewall was made of a long porous lime wood block, in which a big hole serving as the air chamber was drilled along its length. By using an optical microscope, the mean pore diameter of the porous wood was measured to be 35.0 μm. The flow patterns were studied for both vertical and horizontal flows. For the vertical upward flow, the test section orientation is illustrated in Fig. 3(a), while for the horizontal flow the test section was horizontally arranged with the permeable wall as the lower sidewall, as shown in Figs. 2 and 3(b).

2.2. Test loop

Experiments were carried out in the test loop that is schematically shown in Fig. 3. Water, pumped from a water tank, passed through a filter, a control valve, a flow meter, and the test section, and eventually returned to the water tank. A bypass with an adjustable valve, together with the control valve, was used to regulate the water flow rates. Simultaneously, air penetrated through the porous sidewall to the test channel from the air chamber, which was connected to the laboratory compressed air system. After passing through the test section, the air was separated from the air–water mixture and released to the atmosphere. A heat exchanger was immersed into the water tank to compensate for the heat generated during the continuous pumping of water.

The water flow rate through the test section was measured by a turbine-type flow meter (McMillan 101-5) together with a rotameter (GILMONT GF-4542-1225), while the flow rate of air was measured by another rotameter (Omega FL1405). The pressure at the outlet of the air flow meter was measured by a pressure transducer so that the flow rate of the air could be corrected based on the ideal gas equation of state. The temperatures at the outlet of the water and air flow meters were measured by two "T" type thermocouples during the experiments.

2.3. Flow visualization

A high-speed motion analyzer (Kodak Ektapro-1000) combined with a digital video camera (Sony DCR-TRV900E) was employed to visualize and record the flow pattern in the test section. A shoot speed of 3000 frames per second with three split screens per frame, equivalent to a recording rate of 9000 split frames per second, was selected to visualize and record each flow pattern, whereas a speed as low as one frame per second was subsequently selected to playback and analyze the recorded images. A 600-W spotlight (Arrilite 600) was employed to meet the lighting requirement for capturing images at the high shooting speed of 9000 splits frame per second. Since the present test section was too long to be covered fully and distinctly in one frame image with the NAVITAR 6X CCD C-Mount Lens employed in the experiment, the test section was divided into eight equally spaced segments, as designed by S_1 to S_8 in Fig. 2. The flow patterns were visualized by focusing the camera on each segment under identical flow and recording conditions. For the upward flow, both the camera and the spotlight were fixed to a platform lifter with an adjustable elevation, as shown in Fig. 3(a). For the horizontal flow, both the camera and the spotlight were mounted in a horizontal orbit and their desired positions were obtained by sliding them along the orbit, as shown in Fig. 3(b).

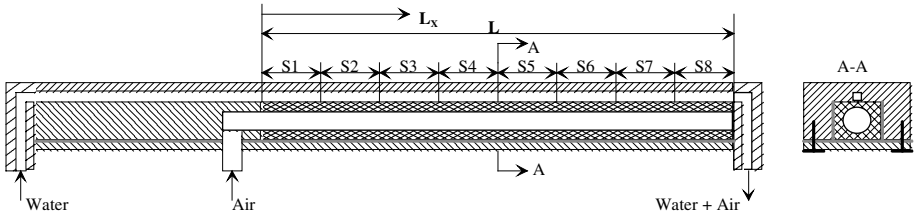

Fig. 2. Schematic of the test channel.

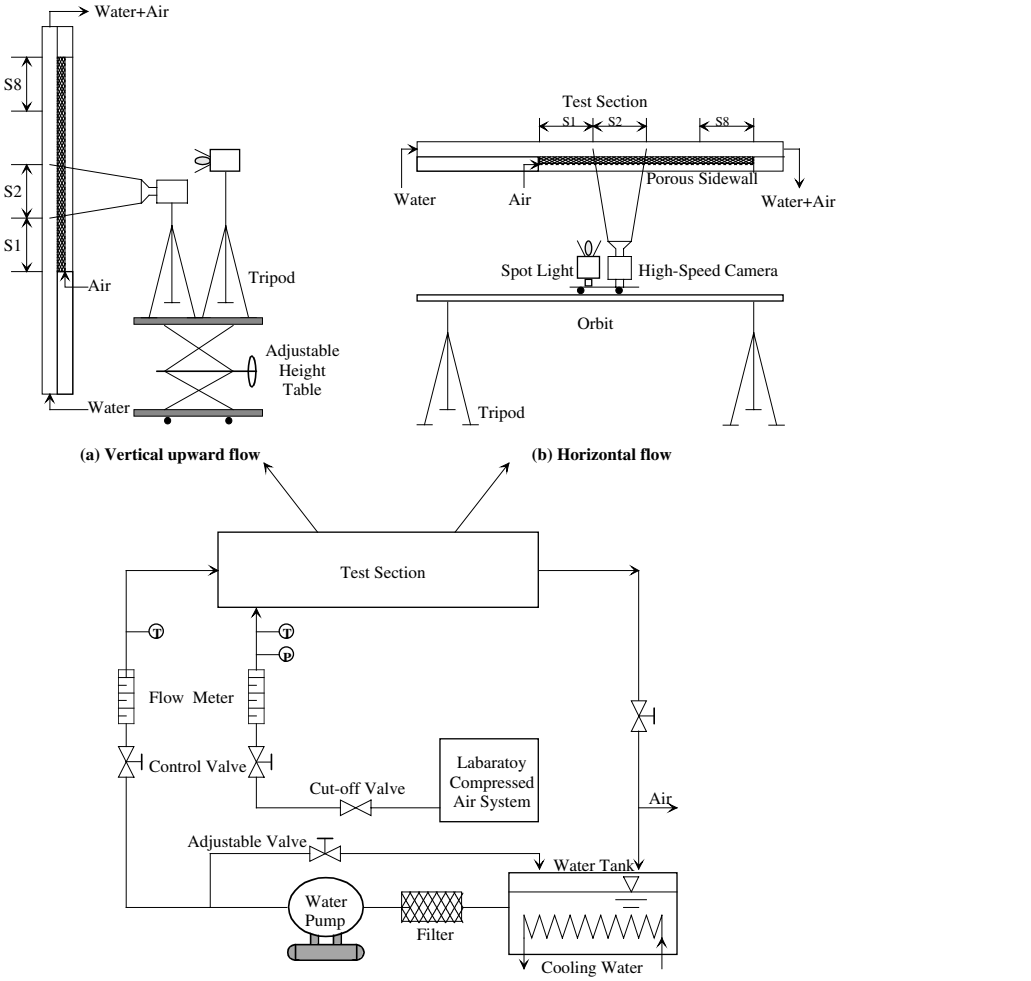

Fig. 3. Schematic of the test facility.

2.4. Flow characterization parameters and test conditions

For the present configured two-phase flow, the flow patterns are characterized by the gas volumetric flux, J_G (m/s) and the liquid volumetric flux J_L (m/s), defined, respectively, as

$$J_G = \frac{Q_G}{A_p} \tag{4}$$

$$J_L = \frac{Q_L}{A_c} \tag{5}$$

where Q_G and Q_L (m^3/s) are the volumetric flow rate of gas and liquid, respectively; A_p is the area of the porous sidewall, and A_c is the cross-sectional area of the channel. As will be seen from the flow patterns presented in latter sections, flow patterns in this work also vary with the mass quality, which increases with channel length. The local mass quality is defined as

$$x = \frac{\rho_G \cdot \frac{Q_G}{L} \cdot L_x}{\rho_L \cdot Q_L + \rho_G \cdot \frac{Q_G}{L} \cdot L_x} \tag{6}$$

where ρ_G and ρ_L are the gas and liquid density, respectively, L_x is the axial distance and $L = 320.0$ mm is the total length of the test section (see Fig. 2). It follows from Eq. (6) that at the entrance of the test section ($L_x = 0$), the mass quality is zero ($x = 0$), while at the exit of the test section ($L_x = L$), the mass quality reaches its maximum value

$$x_{max} = \frac{\rho_G \cdot Q_G}{\rho_L \cdot Q_L + \rho_G \cdot Q_G} \tag{7}$$

Experiments for vertical upward flow were carried out by keeping the volumetric flux of water at $J_L = 0.05$, 0.10, 0.15, 0.20 and 0.25 m/s, respectively, and by varying the volumetric flux of air from 1.33×10^{-2} to 5.568×10^{-2} m/s. For horizontal flow, the volumetric flux of water was kept at $J_L = 0.05$, 0.10, 0.30 and 0.50 m/s, respectively, while the volumetric flux of air varied from 0.1321×10^{-2} to 5.189×10^{-2} m/s. Within the above ranges of the volumetric flux for water and air in both vertical and horizontal flows, the measurements showed that the air was injected uniformly into the test section from the porous sidewall and distinctive flow patterns appeared within the test section.

All the flow patterns in this work were recorded under steady flow state conditions. For a given flow condition, it usually took about half an hour for the flow to reach a steady state condition. For each flow condition, the flow patterns in the eight segments were recorded in a sequence from segments S_1 to S_8 by carefully positioning the camera and the spotlight with the aid of the ruler mounted on the outer surface of the porous sidewall. All the experiments were carried out under conditions of atmospheric pressure (0.1 MPa) and room temperature of 27 °C.

3. Results and discussion

3.1. Flow patterns in vertical upward flow

Figs. 4–6 show the flow patterns observed in vertical upward flow in a channel of 320.0 mm in length for different combinations of the liquid and gas volumetric fluxes. As seen from these figures, typical flow patterns found in vertical upward flow include bubbly flow, slug flow, and annular flow. The features of each flow pattern are described as follows.

Bubbly flow. As shown in Figs. 4–6, bubbly flow can be divided into two stages: "single layer bubbly flow" and "dispersed bubbly flow", although both of them exhibiting the same characteristics, namely that small and spherical gas bubbles are distributed in the continuous liquid phase. As can be seen from the channel entrance region shown in Figs. 4–6, a single layer bubbly flow is distinguished from dispersed bubbly flow by the fact that only a mono small-gas-bubble layer existed adjacent to the surface of the porous sidewall, while the reminding space was still occupied by the liquid phase. It should be pointed out that the formation of a single layer bubbly flow in the present vertical upward

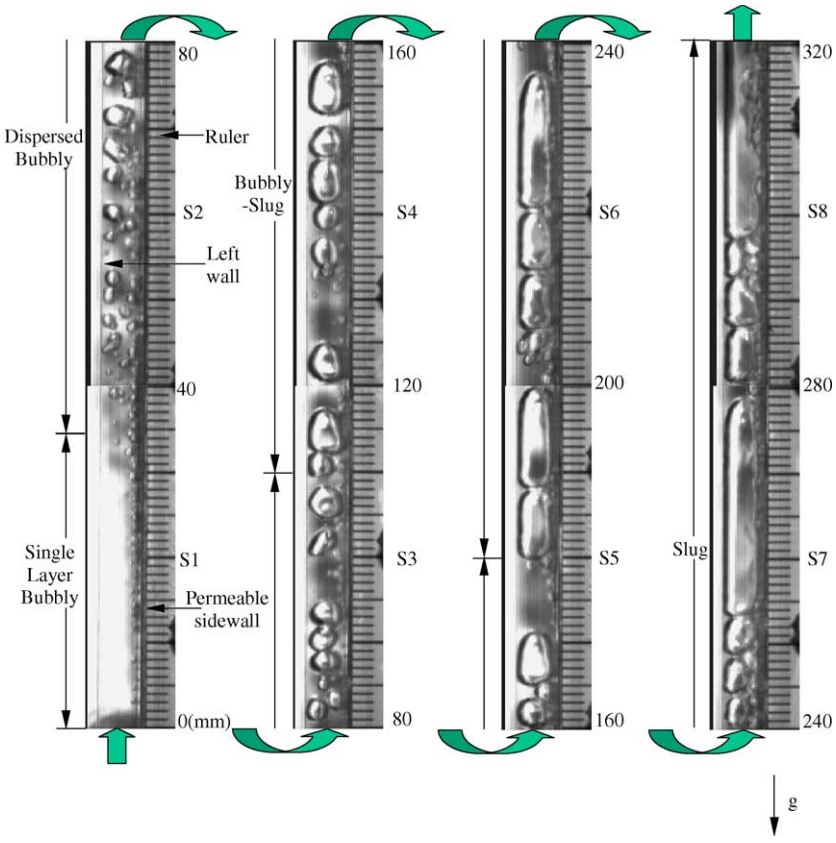

Fig. 4. Flow patterns in vertical upward flow at $J_L = 0.05$ m/s and $J_G = 1.785 \times 10^{-2}$ m/s.

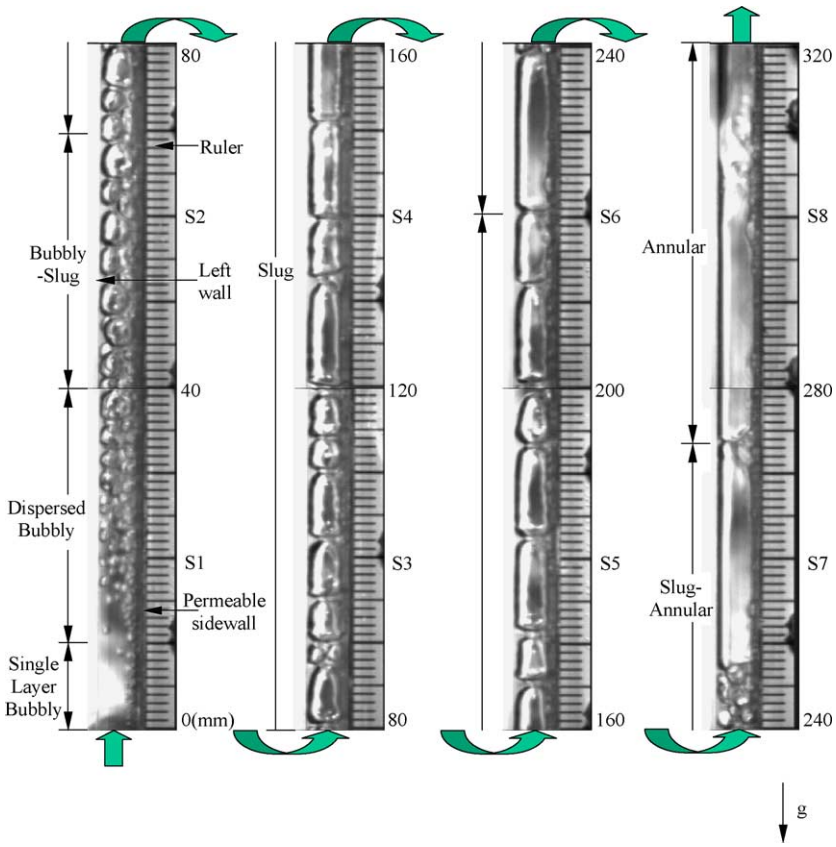

Fig. 5. Flow patterns in vertical upward flow at $J_L = 0.05$ m/s and $J_G = 4.136 \times 10^{-2}$ m/s.

flow is one of the major differences from the conventional co-current two-phase flow. For the present vertical upward flow at low mass quality (in the entrance region), due to the influence of buoyancy, small gas bubbles migrated upward adjacent to the porous sidewall immediately after their departure from the porous surface, forming a single layer of bubbles. With the increase of the mass quality downstream along the channel, the majority of the small bubbles formed in the upstream were pushed toward the liquid core flow by the newly injected bubbles, forming dispersed bubbly flow.

Slug flow. With the effect of the continuous injection of small bubbles from the permeable sidewall, the small bubbles in the dispersed bubbly flow were promoted to coalesce with each other, and some gas slugs were formed, which spanned the entire channel cross-section. As seen from segments S_6 to S_8 in Fig. 4, segments S_3 to S_5 in Fig. 5, as well as segments S_5 and S_6 in Fig. 6, gas slugs are characterized by a semi-spherically shaped nose, an approximately flat tail, and a smooth boundary adjacent to the left channel wall, but a slightly deformed right boundary due to the injection of small bubbles from the permeable sidewall. Some small bubbles existed between two consecutive gas slugs. Further downstream, gas slugs grew in their length direction and became longer and longer. In the meantime, the small bubbles between gas slugs coalesced to form new slugs, and eventually liquid bridges with small bubbles disappeared and slugs got in touch with each other, as shown in segment from S_3 to S_5 in Fig. 5.

Annular flow. For a given volumetric flux of liquid water, an increase in the volumetric flux of gas air will eventually lead to the presence of annular flow, with most of the liquid flowing along the channel wall while the gas flows in the central core, as can be seen from segment S_8 in Figs. 5 and 6. The left liquid film profile of annular flow was more or less the same as that in the conventional co-current two-phase upward flow in a vertical channel. However, a distinct feature of annular flow for the present flow configuration is that small bubbles were continuously generated from the porous sidewall, and grew by blowing up the liquid film to form a semi-sphere shape, and then ruptured and released gas into the core flow. As a result, the liquid film profile at the right side was significantly deformed by the continuous injection of gas bubbles from the porous sidewall. During the period of blowing up the liquid film, the surface of the porous plate under the

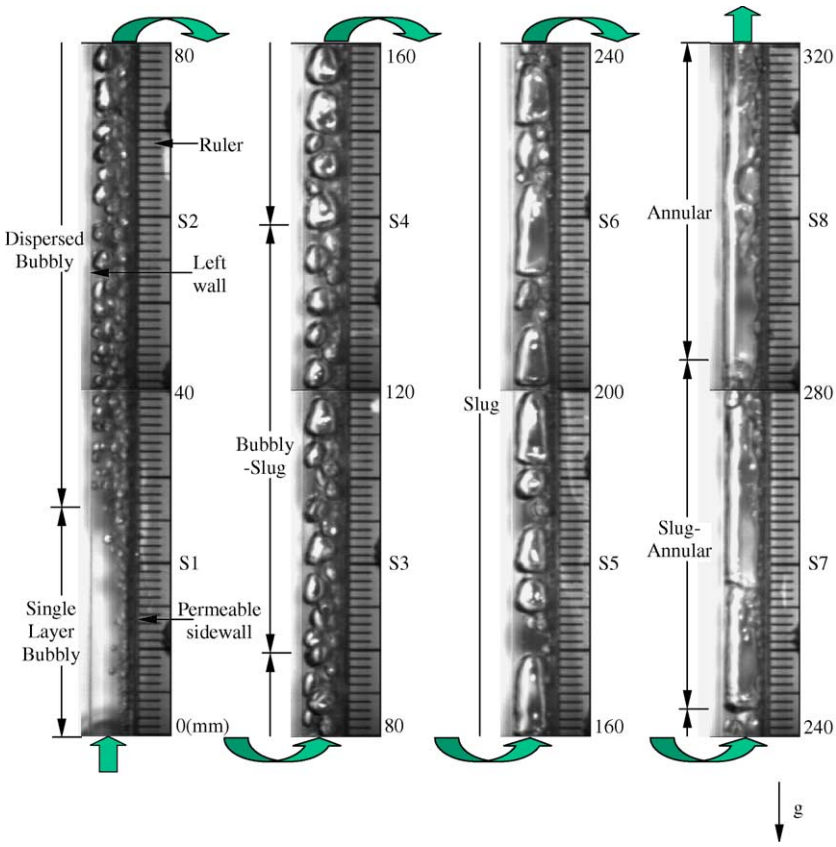

Fig. 6. Flow patterns in vertical upward flow at $J_L = 0.10\,m/s$ and $J_G = 4.149 \times 10^{-2}\,m/s$.

semi-sphere film is periodically isolated from the liquid phase. When this phenomenon appears in the flow passages of a DMFC, it means that the liquid fuel cannot be quickly and continuously transported to the electrochemical reaction side through the surface of gas diffusion layer, leading to concentration polarization and deteriorating in the fuel cell performance. Thus, annular flow should be avoided during the operation of a DMFC.

In summary, for the present flow configured gas–liquid two-phase vertical upward flow, various flow patterns appeared in the channel from its entrance to its exit in a sequence of single layer bubbly flow, dispersed bubbly flow, slug flow, and annular flow, as the mass quality increased along the test channel. The length of each flow pattern varied with the volumetric fluxes of liquid and gas. A comparison between Figs. 4 and 5 indicates that for a given liquid volumetric flux, the space occupied by each flow pattern became shorter with an increase in the gas volumetric flux. Similarly, a comparison between Figs. 5 and 6 indicates that for approximately the same air volumetric flux, the space occupied by each flow pattern became longer with an increase in the liquid water volumetric flux. This behavior suggests that an increase in the liquid fuel volumetric flux is one of the most effective measures to avoid annular flow appearing inside the anode channels in a DMFC.

In addition to the various distinct flow patterns described above, some transitional flow patterns, such as bubbly-slug flow, and slug-annular flow in the vertical upward flow were also observed between two distinct flow patterns, as indicated in Figs. 4–6. During the experiments, we observed that in the locations where a transitional flow pattern occurred two distinct flow patterns (bubbly and slug flow, slug and annular flow) appeared alternately. For instance, for bubbly-slug flow, bubbly flow and slug flow occurred at the same location alternately and the flow at this location can neither be classified as bubbly flow nor as slug flow. The presence of the transitional flow patterns resulted from a periodic bubble growth and departure along the porous sidewall. This periodic bubble growth and departure lead to a slow process for one distinct flow pattern to transition to another. However, it is worth pointing out that the slug-annular flow found in this work was to some extent like the churn flow encountered in conventional co-current liquid–gas two-phase vertical upward flow.

3.2. Flow patterns in horizontal flow

The flow patterns found in horizontal flow for different combinations of the liquid and gas volumetric fluxes are shown in Figs. 7–9. The characteristics of the typical flow patterns in horizontal flow, including bubbly flow, plug flow, slug flow, and annular flow are described as follows.

Bubbly flow. As seen from Figs. 7–9, bubbly flow, characterized by the presence of small discrete bubbles in the continuous liquid phase, usually occurred in the entrance region, i.e.: segment S_1 although it was sometimes observed within segments S_2 for low volumetric fluxes of air and high volumetric fluxes of water (see Fig. 9). Compared to the bubbly flow pattern encountered in the conventional co-current two-phase flow in a channel with a well-mixed gas–liquid mixture entering the channel, one of the most distinct features of the present configured flow is that, owing to the effect of buoyancy, small bubbles injected from the lower permeable wall traveled upwards to the upper portion of the channel, where relatively large bubbles were formed due to collision and coalescence of small ones.

Plug flow. Immediately after the bubbly flow region, plug flow was observed at low volumetric fluxes, like the flow condition of $J_L = 0.1$ m/s and $J_G = 0.8551 \times 10^{-2}$ m/s shown in segment S_3 and partial portion of segment S_4 in Fig. 7. These plug bubbles are characterized by a flat-shaped top adjacent to the upper channel wall, a semi-sphere bottom, and a large axial length, but the radial size of the plug bubbles is usually too small to span the channel cross-section. It is also observed that some tiny discrete bubbles usually existed between two adjacent large plug bubbles and under plug bubbles. The formation of plug flow was due to the fact that small bubbles in the bubbly flow regions continuously collided with the bubbles entering from the surface of the lower

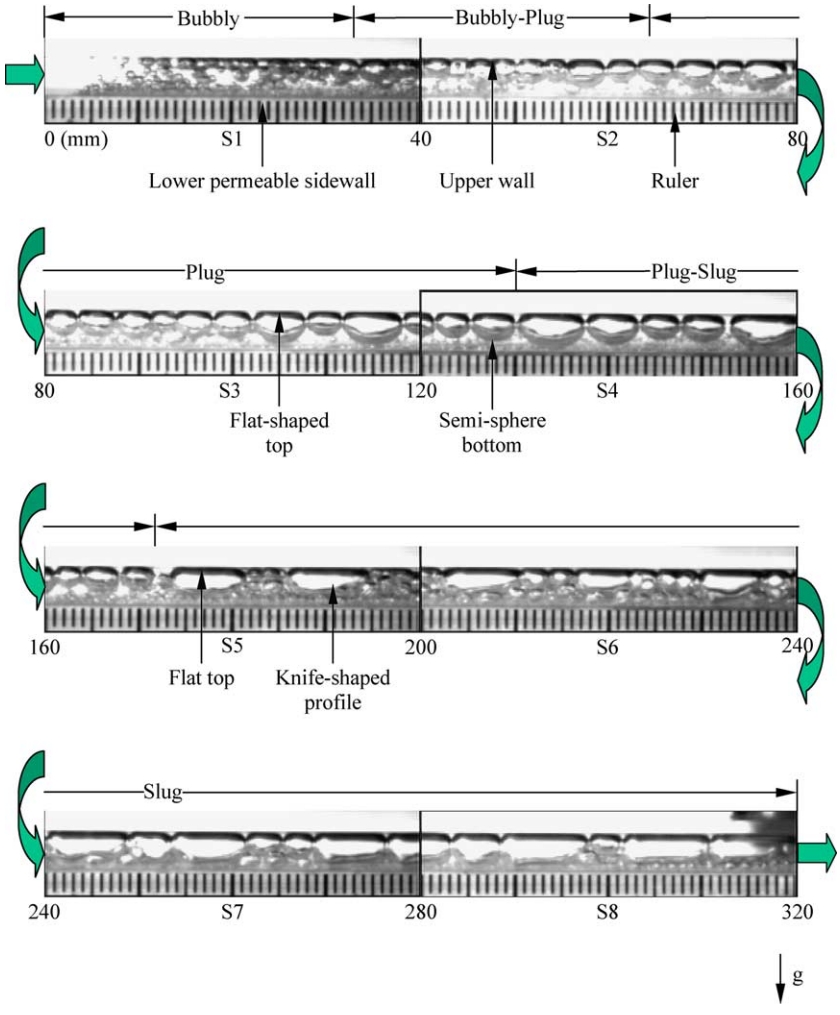

Fig. 7. Flow patterns in horizontal flow at $J_L = 0.10$ m/s and $J_G = 0.8551 \times 10^{-2}$ m/s.

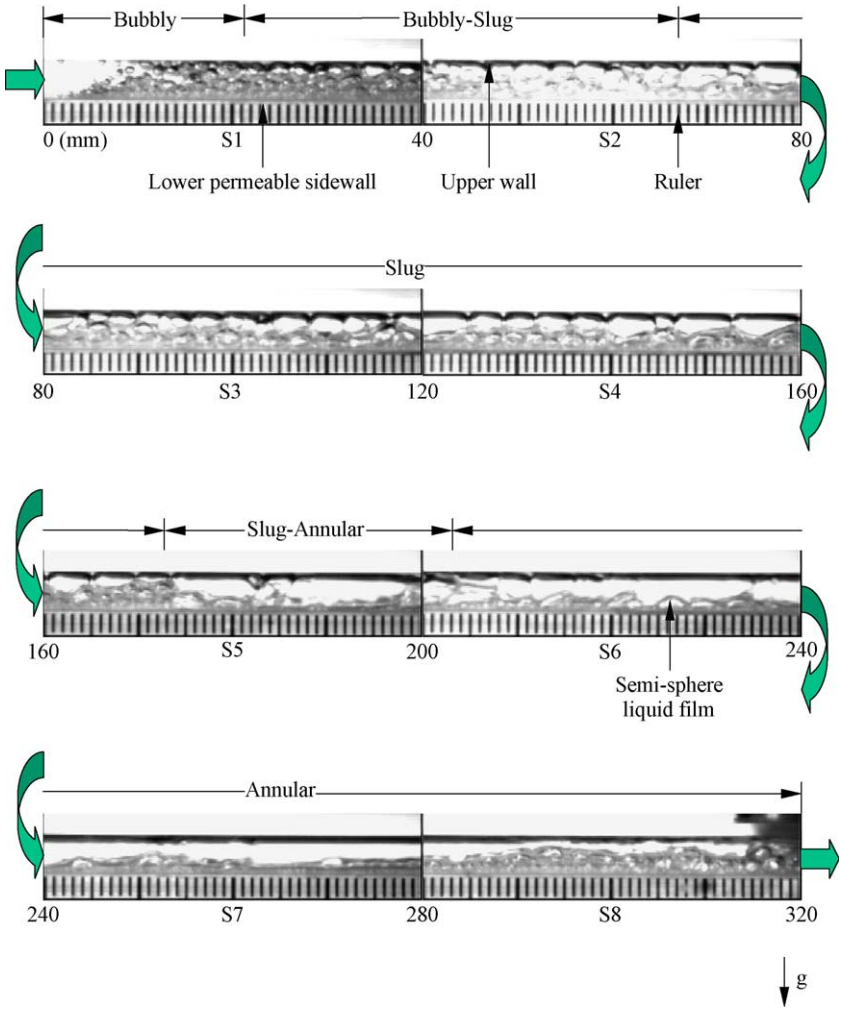

Fig. 8. Flow patterns in horizontal flow at $J_L = 0.10\,m/s$ and $J_G = 4.02 \times 10^{-2}\,m/s$.

permeable wall. It should be noted that at high air volumetric fluxes, as seen from Fig. 8 ($J_G = 4.02 \times 10^{-2}$ m/s) and Fig. 9 ($J_G = 4.033 \times 10^{-2}$ m/s), plug flow disappeared from the test section and bubbly flow transitioned to slug flow directly. This can be attributed to the fact that the high density of bubbles nucleating at the surface of the permeable sidewall at the high air volumetric flux, causing small bubbles to quickly coalesce with each other and grow fast enough to become slug bubbles directly.

Slug flow. As seen from Fig. 7, the plug bubbles further downstream changed to large slug bubbles with the addition of small bubbles injected from the lower permeable wall. Under the condition of high air volumetric fluxes, as shown in Figs. 8 and 9, small bubbles directly transitioned to slug bubbles without intermediate plug bubbles for the case with low air volumetric fluxes shown in Fig. 7. Slug bubbles, as seen in segments S_5 to S_8 in Fig. 7, segments S_3 and S_4 in Fig. 8, as well as segments S_4 and S_5 in Fig. 9, usually had a knife-shaped profile, flat at their top portions and narrow at their caps. Unlike plug bubbles, slug bubbles had a much larger radial size and almost spanned the entire cross-section of the flow channel. Because of buoyancy, the slugs of gas flowing along the channel tended to skew toward the upper portion of the channel. Similar to the vertical upward flow, some middle-sized bubbles could often be observed between two consecutive slugs, while small bubbles generated from the surface of the lower porous sidewall resulted in a slight deformation in the lower boundaries of the gas slugs. As seen from Figs. 7 and 8, for the same water flow rate, slug flow usually occurred in the downstream portion of the channel at low volumetric fluxes of air (e.g.: $J_G = 0.8851 \times 10^{-2}$ m/s), but in the middle of the channel at high volumetric fluxes of air (e.g.:. $J_G = 4.02 \times 10^{-2}$ m/s).

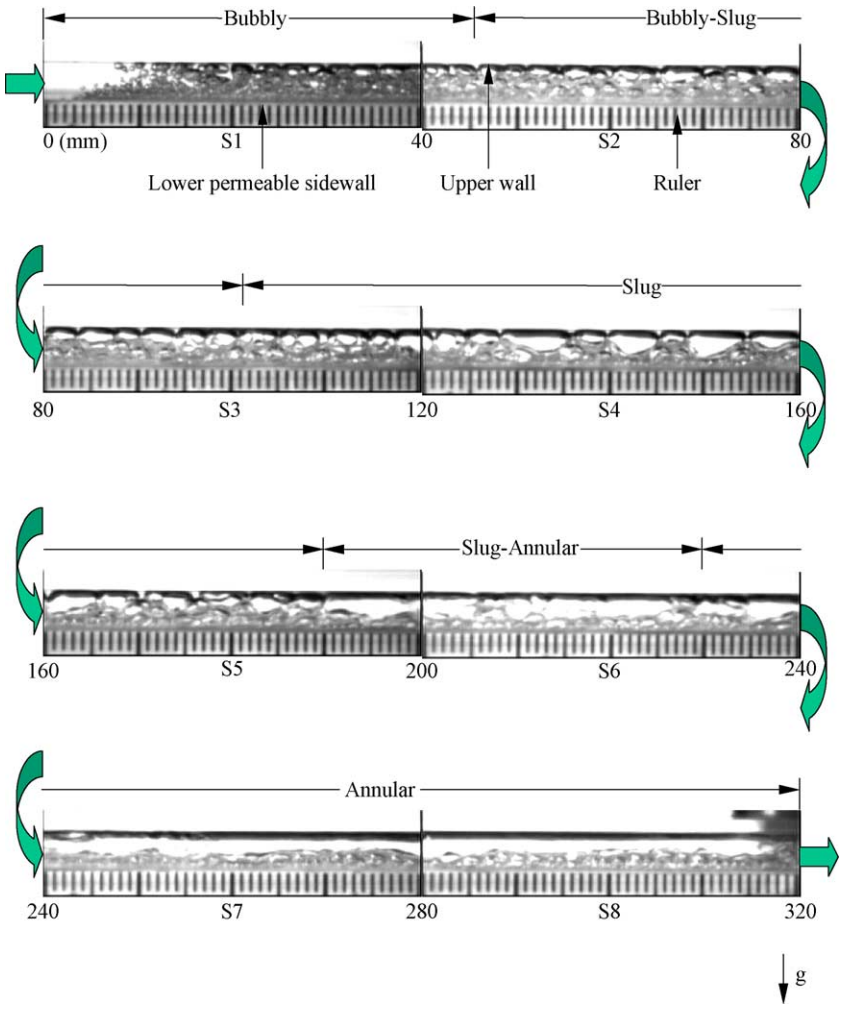

Fig. 9. Flow patterns in horizontal flow at $J_L = 0.30\,m/s$ and $J_G = 4.033 \times 10^{-2}\,m/s$.

Annular flow. Annular flow in the horizontal flow has more or less the same features as in the vertical upward flow, where most of the liquid flows along the channel wall while the gas flows in the central core. As can be seen from segments S_6 to S_8 in Fig. 8 and from segments S_7 and S_8 in Fig. 9, small bubbles were continuously generated from the lower permeable wall where they grew bigger by blowing up the lower liquid film, forming a semi-sphere shape and then rupturing and releasing gas into the core flow. As a result, the lower liquid film profile was significantly deformed by the continuous injection of gas bubbles from the lower porous wall.

In summary, for the present flow configured gas–liquid two-phase horizontal flow, various flow patterns appeared in the channel from its entrance to its exit in a sequence of bubbly flow, plug flow, slug flow, and annular flow, as the mass quality increased along the test channel. It is worth mentioning that at high air volumetric fluxes, plug flow disappeared from the test section and bubbly flow transitioned to slug flow directly. Similar to the vertical upward flow, the length of each flow pattern varied with the volumetric fluxes of liquid and gas. A comparison between Figs. 7 and 8 indicates that for a given liquid volumetric flux, the space occupied by each flow pattern became shorter with an increase in the gas volumetric flux. Similarly, a comparison between Figs. 8 and 9 indicates that for approximately the same gas volumetric flux, the space occupied by each flow pattern became longer with an increase in the liquid volumetric flux.

In addition to the various distinct flow patterns described above, some transitional flow patterns, similar to the vertical upward flow, were also observed between two distinct flow patterns. As indicated in Figs. 7–9, these transitional flow patterns include bubbly-plug flow, plug–slug flow, bubbly-slug flow and slug-annular flow.

Comparing the flow patterns in the vertical upward flow (Figs. 4–6) and in the horizontal flow (Figs. 7–9), one of the major differences is that there is a tendency to create stratification of the flow due to the influence of buoyancy. As can be observed from Figs. 7–9, the gas tended to migrate toward the top of the channel while the lower portion of the channel carried more of the liquid with the bottom of the channel full of small gas bubbles. Comparing Fig. 6 with Fig. 8, it can be seen that, because of the influence of buoyancy, the regime

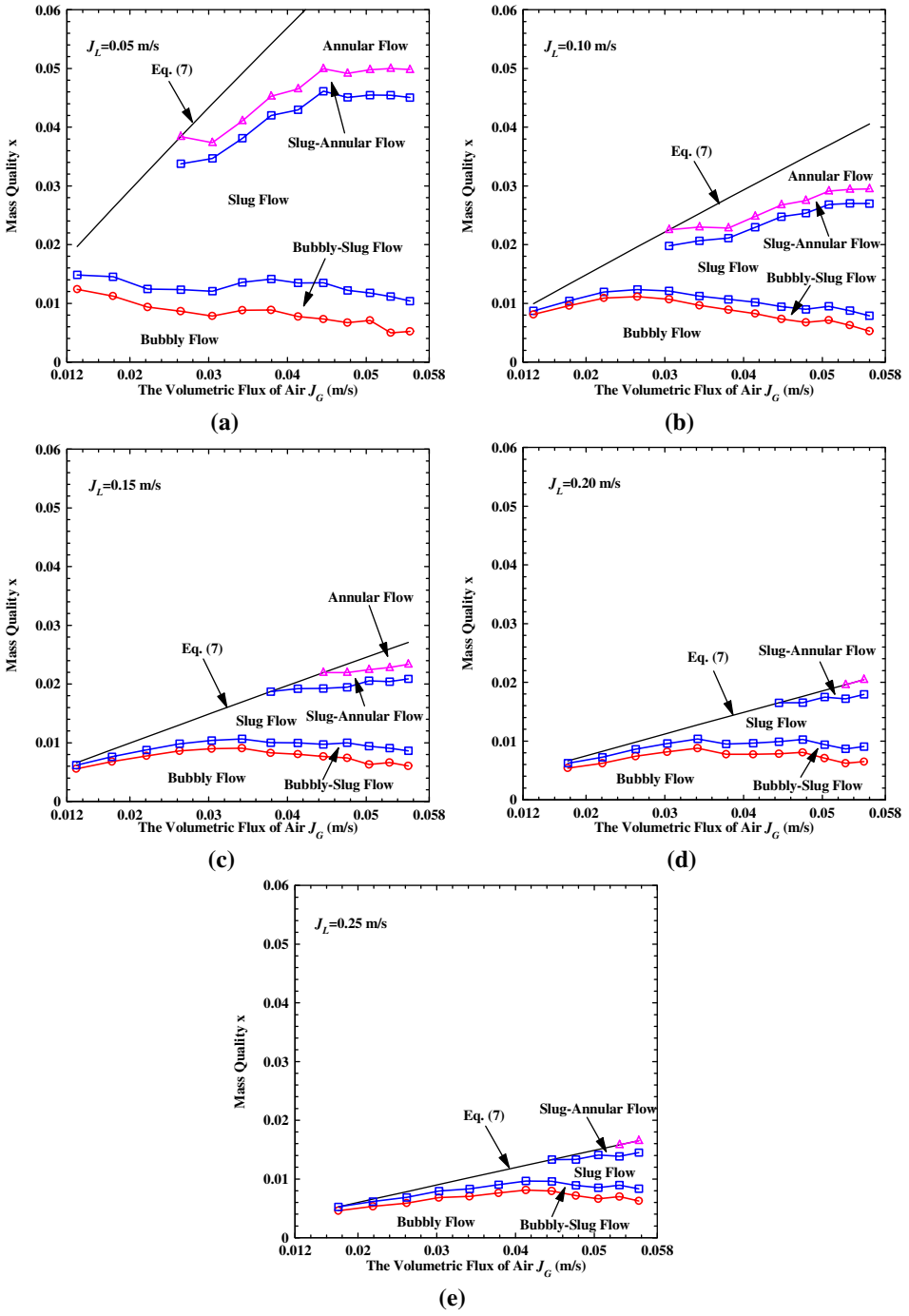

Fig. 10. Flow regime maps for vertical upward flow.

for each flow pattern in the vertical upward flow was much longer than that in the horizontal flow for approximately the same volumetric fluxes of water and air.

3.3. Flow regime maps

In the conventional co-current gas–liquid two-phase flow, flow patterns were presented in 2-D flow maps by using various parameters. For instance, Baker [18] presented the flow pattern map for horizontal flow by using (G_g/λ) and $(G_f\psi)$, where G_g and G_f are the superficial mass velocity of the gas and liquid phases, respectively, and the factors λ and ψ are given by

$$\lambda = \left[\left(\frac{\rho_g}{\rho_A}\right)\left(\frac{\rho_f}{\rho_W}\right)\right]^{1/2} \tag{8}$$

and

$$\psi = \left(\frac{\sigma_W}{\sigma}\right)\left[\left(\frac{\mu_f}{\mu_W}\right)\left(\frac{\rho_W}{\rho_f}\right)^2\right]^{1/3} \tag{9}$$

Hewitt and Roberts [1] presented the flow pattern map for vertical flow by using the superficial momentum fluxes of the liquid $(\rho_f J_f^2)$ and gas $(\rho_G J_G^2)$. Other previous investigators, for instance, Zhao and Bi [13], and Kawahara et al. [19], used the liquid and gas volumetric flux (J_L) and gas (J_G) to characterize the flow patterns in a 2-D flow map. For the present configured two-phase flow, since the flow patterns varied with the mass quality along the channel length in addition to the liquid and gas volumetric fluxes, we present the flow patterns in terms of the volumetric flux of gas and the mass quality for a given volumetric flux of liquid in Figs. 10 and 11. The boundaries between the flow regimes were established from visual observation of the two-phase flow in a series of experiments by varying the volumetric flux of air at a fixed volumetric flux of water. The mass quality x was determined from Eq. (6), in which $L_{x,s}$ and $L_{x,e}$ are substituted for L_x, with $L_{x,s}$ and $L_{x,e}$ representing, respectively, the locations of the starting point and the end point of each specific flow pattern. $L_{x,s}$ and $L_{x,e}$ of each flow pattern were measured with the aid of the ruler

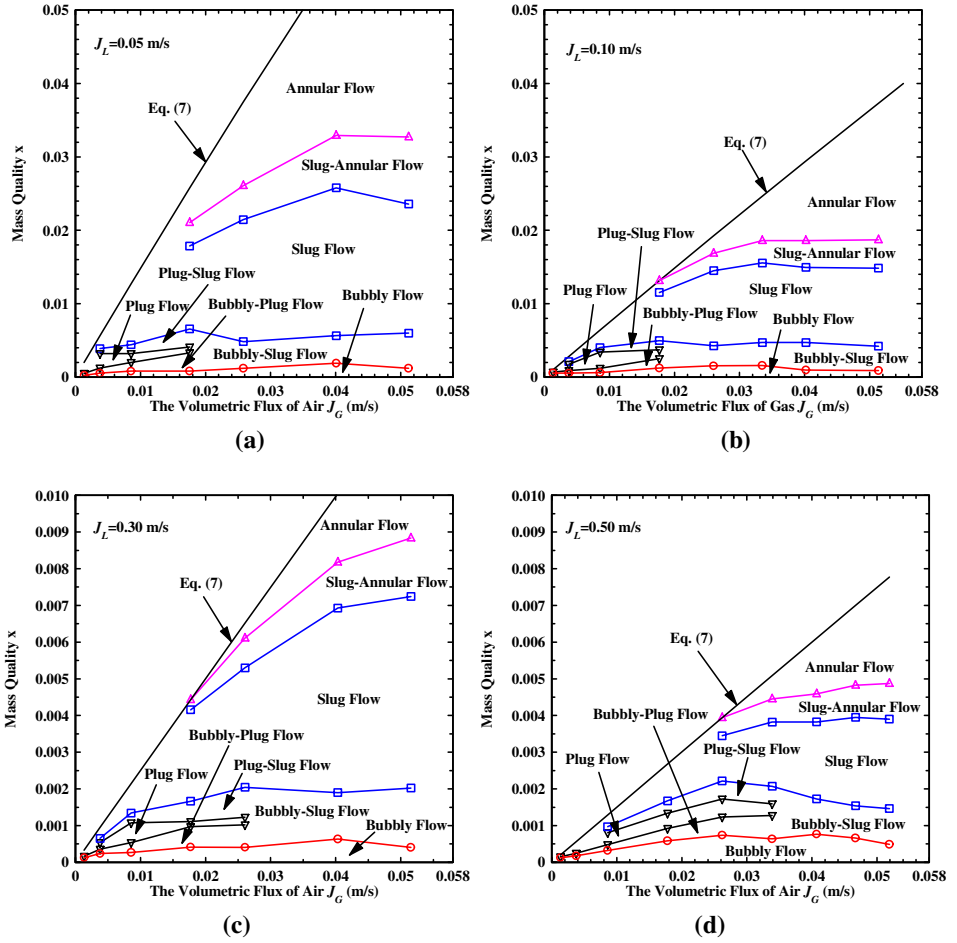

Fig. 11. Flow regime maps for horizontal flow.

attached to the outer surface of the porous block. It is worth mentioning that for given volumetric fluxes of water and air the mass quality varied from zero to x_{max}, given by Eq. (7), corresponding to the exit of the test section.

The flow regime maps for vertical upward flow at selected volumetric fluxes of water (0.05, 0.10, 0.15, 0.20, and 0.25 m/s) are presented in Fig. 10(a)–(e), respectively. As can be seen from Fig. 10(a)–(c) for low volumetric fluxes of water, at high volumetric fluxes of air (see the horizontal coordinate), with an increase in the mass quality (the vertical coordinate) the flow regimes typically appear in the sequence of bubbly flow, bubbly-slug flow, slug flow, slug-annular flow, and annular flow. However, at low volumetric fluxes of air, Fig. 10(a)–(c) indicate that some flow patterns such as slug flow and annular flow may never appear in the channel. For the cases of high volumetric fluxes of water shown in Fig. 10(d) and (e), annular flow pattern never appeared in the entire channel over the range of the volumetric flux of air, although bubbly flow and slug flow were always encountered. In addition, a progressive scan of five flow regime maps for vertical upward flow from Fig. 10(a)–(e) indicated that both the bubbly-slug transition flow area and the slug-annular transition flow area shifted downward, as the mass quality was reduced.

Fig. 11(a)–(d) presents the flow regime maps for horizontal flow at selected volumetric fluxes of water (0.05, 0.10, 0.3, and 0.50 m/s). In general, the flow regime transition behaviors for horizontal flow are similar to those described above for vertical upward flow. One feature that is different from vertical upward flow is that plug flow occurs at low volumetric fluxes of air, but it disappeared as the volumetric flux of air reached a critical value. As can been seen from Fig. 11(a)–(d), this critical value increased from 1.8×10^{-2} m/s to 3.4×10^{-2} m/s with the increase in the volumetric flux of water from 0.05 m/s to 0.50 m/s.

4. Concluding remarks

A visual investigation of liquid–gas two-phase flow in a miniature square cross-section channel ($d_h = 5.0$ mm) having a permeable sidewall has been performed. It has been shown that the typical flow patterns, encountered in the conventional co-current gas–liquid two-phase flow, such as bubbly flow, plug flow, slug flow, and annular flow, were also found in this work. However, due to the special flow configuration considered in this work, stratified flow, characterized by the fact that the two phases flow separately with a relatively smooth interface in the conventional co-current two-phase horizontal flow, was not found in present horizontal flow. And a so-called single layer bubbly flow, characterized by a mono small-gas-bubble layer existed adjacent to the surface of permeable sidewall while the remaining space occupied by the liquid phase, was found in the present vertical upward flow at a lower volumetric flux of air. It was also found that some new characteristics were presented in these typical flow patterns. For example, slug bubbles have a slightly deformed boundary for the lower boundary in the horizontal flow and for the right boundary in the vertical upward flow. In the annular flow, small bubbles were continuously generated from the porous sidewall, which grew by blowing up the liquid film, forming a semi-sphere shape, and then rupturing and releasing gas into the core flow. The characteristics of the annular flow found in the present work suggest that annular flow appearing inside the anode channels of a DMFC should be avoided, as it may deteriorate the fuel cell performance. The experiments show that one of the most effective measures to avoid the presence of annular flow is to increase the liquid volumetric flux. Furthermore, four transition flow patterns, bubbly-plug flow, bubbly-slug flow, plug–slug flow, and slug-annular flow, were observed and recorded. Finally, flow regime maps have been developed in the term of the volumetric flux of the gas phase and the mass quality for each given liquid phase volumetric flux.

Acknowledgments

The work described in this paper was fully supported by a grant from the Research Grants Council of the Hong Kong Special Administrative Region, China (project no. HKUST6178/00E).

References

[1] G.F. Hewitt, D.N. Roberts, Studies of two-phase flow patterns by simultaneous X-ray and flash photography, AERE-M 2159 (1969), HMSO.
[2] G.E. Alves, Co-current liquid–gas flow in a pipeline contactor, Chen. Process. Eng. 50 (9) (1954) 449–456.
[3] L.P. Golan, A.H. Stenning, Two-phase vertical flow maps. Paper No. 14 presented at Symposium on Fluid Mechanics and Measurements in Two-phase Flow Systems, Leeds University, 1969, pp. 24–25.
[4] T. Oshinowo, M.E. Charles, Vertical two-phase flow. Part I. Flow pattern correlations, Can. J. Chem. Eng. 52 (1974) 25–35.
[5] S.I. Kosterin, An investigation of the influence of the diameter and inclination of a tube on the hydraulic resistance and flow structure of gas–liquid mixtures, Izvest. Akad. Nauk. S.S.S.R. Otdel Tekh. Nauk 12 (1949) 1824.
[6] W.E. Brigham, E.D. Holstein, R.L. Huntington, Two-phase concurrent flow of liquids and air though inclined pipe, Oil Gas J. 11 (1957) 145.
[7] C. Damianides, Horizontal two-phase flow of air-water mixtures in small diameter tubes and compact heat

exchangers. Ph.D. Dissertation, University of Illinois at Urbana-Champaign, 1987.
[8] K. Mishima, T. Hibiki, Some characteristics of air–water two-phase flow in small diameter vertical tubes, Int. J. Multiphase Flow 22 (1996) 703–712.
[9] L. Galbiati, P. Andreini, Flow pattern transition for vertical downward two-phase flow in capillary tubes, inlet mixing effects, Int. Commun. Heat Mass Transfer 19 (1992) 791–799.
[10] J.K. Keska, R.D. Fernando, Average physical parameters in an air–water two-phase flow in a small square-section channel, J. Fluids Eng.—Trans. ASME 116 (1994) 247–256.
[11] J.W. Coleman, S. Garimella, Characterization of two-phase flow patterns in small diameter round and rectangular tubes, Int. J. Heat and Mass Transfer 42 (1999) 2869–2881.
[12] M.E. Ewing, J.J. Weinandy, R.N. Christensen, Observations of two-phase flow patterns in a horizontal circular channel, Heat Transfer Eng. 20 (1) (1999).
[13] T.S. Zhao, Q.C. Bi, Co-current air–water two-phase flow patterns in vertical triangular microchannels, Int. J. Multiphase Flow 27 (2001) 765–782.
[14] K.A. Triplett, S.M. Ghiaasiann, S.I. Abdel-Khalik, D.L. Sadowski, Gas–liquid two-phase flow in microchannels. Part I: Two-phase flow patterns, Int. J. Multiphase Flow 25 (1999) 377–394.
[15] M.M. Mech, S. Boslet, S. Thynell, J. Scott, C.Y. Wang, Experimental study of a direct methanol fuel cell, in: Proceedings of the Symposium on Direct Methanol Fuel Cells, the 199th Electrochemical Society Proceedings Series, Princeton, NJ, 2001.
[16] P. Argyropoulos, K. Scott, W.M. Taama, Carbon dioxide evolution patterns in direct methanol fuel cells, Electrochim. Acta 44 (1999) 3575–3584.
[17] H. Yang, T.S. Zhao, P. Cheng, Characteristics of gas–liquid two-phase flow patterns in miniature channel having a gas permeable sidewall, 2002 International Mechanical Engineering Congress and Exhibition, New Orleans, USA, November, 2002, pp. 17–22. Paper No. IMECE2002-32542.
[18] O. Baker, Design of pipe lines for simultaneous flow of oil and gas, Oil Gas J. 26 (July) (1954) 185–190, 192, 195.
[19] A. Kawahara, P.M.-Y. Chung, M. Kawaji, Investigation of two-phase flow pattern, void fraction and pressure drop in a microchannel, Int. J. Multiphase Flow 28 (2002) 1411–1435.